ACS Photonics

Article

pubs.acs.org/journal/apchd5

Graphene/PbS as a Novel Counter Electrode for Quantum Dot Sensitized Solar Cells

Parisa Parand,[†] Mahmoud Samadpour,*[,†] Ali Esfandiar,[‡] and Azam Iraji Zad*[,§]

[†]Department of Physics, K.N. Toosi University of Technology, PO Box 15418-49611, Tehran, Iran

[‡]Department of Physics, Kharazmi University, PO Box 1571914911, Tehran, Iran

[§]Institute for Nanoscience and Nanotechnology, Sharif University of Technology, P.O. Box 11155-8639, Tehran, Iran

ABSTRACT: PbS nanoparticles were *in situ* deposited on graphene sheets by a successive ionic liquid adsorption and reaction method to prepare a graphene/PbS composite counter electrode for CdS/CdSe quantum dot sensitized solar cells (QDSCs). Under 1 sun illumination, the cells with graphene/PbS counter electrodes (CEs) show a maximum energy conversion efficiency of 2.63%, which is remarkably higher than that of those employing PbS (1.28%) or graphene (0.23%) CEs. Electrochemical impedance spectroscopy analysis shows that graphene/PbS composite counter electrodes have lower charge-transfer resistance at the interface of the CE and the polysulfide redox electrolyte, compared to those cells with PbS and graphene counter electrodes. For the first reported CdS/CdSe-sensitized cells with the G/PbS CE, a cell performance with 2.63% efficiency (V_{oc} = 559 mV, J_{sc} = 11 mA/cm^2, FF = 0.42) was obtained, which is comparable with the photovoltaic properties of the cells with optimized conventional Cu_2S CEs (η = 3.01%, V_{oc} = 564 mV, J_{sc} = 11.6 mA/cm^2, FF = 0.46). Our results indicate the potential application of graphene/noble metal sulfide composite electrodes in high-efficiency QDSCs.

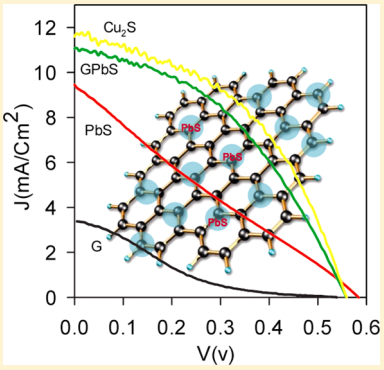

KEYWORDS: *solar cell, quantum dot, graphene, PbS, counter electrode*

Dye-sensitized solar cells (DSCs) are of great interest due to their simple fabrication procedure and rather high efficiencies. Beside DSCs, recently inorganic semiconductors have received a great deal of attention as alternative sensitizers to dye molecules. They are used instead of dyes in the same configuration of DSCs in order to make quantum dot sensitized solar cells (QDSCs).[1−7] Quantum dots exhibit unique properties such as high molar extinction coefficients, easy fabrication, and a tunable absorption spectrum by controlling their size and composition.[4] In the past few years, there has been a considerable effort to push up the energy conversion efficiencies of QDSCs by using various strategies. A review of the literature indicates that much of the research in QDSCs has focused on synthesis of various structures of photoanodes,[8−11] sensitizing the photoanodes with various combinations of QDs,[12,13] depositing QDs on an anode with various chemical methods,[13,14] and changing the chemical composition of the redox electrolyte.[15−19] For example, Sudhagar et al. obtained as high as 750 mV open-circuit photovoltage by synthesis of various structures of a photoanode.[9] More than 18.4 mA/cm^2 current density has been obtained by modifying both QD preparation methods and sensitizing the photoanode with various combinations of QDs.[20] In spite of the comparable open-circuit voltages and current densities in QDSCs and DSCs,[9,20] their fill factor (less than 0.6)[21,22] is considerably lower than DSCs, which is typically more than 0.7.[23,24]

It is known that the series resistance in both DSCs and QDSCs is one of the main parameters that noticeably affect the fill factor. For example annealing the active layer can improve the electrical connectivity between TiO_2 nanoparticles and between nanoparticles and the FTO glass substrate. Therefore the improved conductivity in the active layer decreases the series resistance of the cells and consequently improves the fill factor. In addition to the properties of the active layer, kinetics of the charge transfer at the CE/electrolyte interface affects the fill factor in a clear way. Considerable obscurity in charge transfer at the counter electrode (CE)/electrolyte interface increases the internal resistance and concentration gradients of the redox species in the electrolyte, parameters that strongly affect the fill factor. So various optimizations need to be done in order to boost the fill factor and the efficiency of the cells. A review of the literature indicates that in spite of various optimizations done on the active layer,[8−11] finding a suitable CE with good charge transfer at the CE/electrolyte interface is still a challenge in QDSCs.

Therefore the introduction of new CE materials with improved catalytic activities could lead to comparable or even better fill factors in QDSCs than DSCs. Currently various CEs such as Cu_2S, CoS, PbS, Au, and Pt[21,25−27] are generally used in QDSCs, but the electrocatalytic properties of these are considerably less than the catalytic properties of the CEs, which are normally used in DSCs.[23,24] Currently DSCs normally use the Pt CE, which has considerable catalytic activity in polyiodide redox electrolytes. Using Pt CEs, fill factors of more

Received: August 23, 2013
Published: March 24, 2014

 © 2014 American Chemical Society

than 0.7 are usually obtained in DSCs. In spite of the good catalytic properties of Pt in a polyiodide electrolyte, it has a weak catalytic activity in a polysulfide redox electrolyte and more importantly is not chemically stable in this electrolyte. In spite of the intrinsic catalytic activity of Cu_2S, CoS, and PbS in a polysulfide redox electrolyte, charge carrier mobility is not significant in these CEs. It seems that a noticeable improvement in cell efficiencies can be obtained by compositing these CEs with more conductive materials that have good chemical stability in redox polysulfide electrolytes.

There are several parameters that affect the CE performance noticeably. The first is the good conductivity of the CE, which improves the charge transport to the active catalyst sites in the CE. The second parameter is the amount of the CE catalytic activity that influences the reduction rate of the oxidized species in the redox electrolyte. The last parameter is the amount of effective interface area between the CE and redox electrolyte.

Recently carbon nanostructures, such as carbon nanotubes, graphene (G), and other carbon derivatives, have received more attention as a conductive support or catalyst in DSCs and in some cases in QDSCs.[28−34] Among the carbon nanostructures, graphene has attracted much research attention due to its excellent properties such as high charge carrier mobility, catalytic activity, and chemical stability, enabling application in catalysis and energy storage.[35]

A literature review indicates that carbon nanostructures have good chemical stability in polysulfide redox electrolytes.[34] In spite of the inherent chemical stability and good conductivity of graphene, its catalytic activity should be improved by surface functionalization or decoration by more catalytic quantum dots. Here, regarding the high conductivity and chemical stability of graphene and good catalytic activities of the PbS QDs, considerable improvement in catalytic properties could be expected by compositing graphene and PbS nanoparticles.

Regarding the unique properties of graphene, here as an alternative novel CE, composite graphene (G)/PbS has been applied to fabricate CdS/CdSe-sensitized solar cells. Besides the G/PbS composite electrode, QDSCs were also prepared using graphene, PbS, and Cu_2S counter electrodes for comparison. Basic $J-V$ characteristics were measured under AM1.5 standard simulative solar light of 100 mW cm^{-2} to compare the performance of cells with different CEs. Electrochemical impedance spectroscopy (EIS) was employed to study and compare the catalytic properties of various CEs. In the present study, we show that composites of noble metal sulfides and graphene have considerable catalytic activities for application in QDSCs.

EXPERIMENTAL SECTION

Preparation of the TiO_2 Photoanode. Two different TiO_2 commercial pastes were obtained from Dyesol: DSL-18NR-T (TiO_2 particle size 20 nm) and DSL-18NR-AO (TiO_2 particle size 20−450 nm). The first paste produces electrodes with a high effective surface area, while the other one is commonly employed as a light-scattering layer in DSCs and QDSCs. All the photoanodes were prepared by doctor-blading a single layer of each paste on transparent conducting fluorine doped tin oxide (FTO) glass substrates (sheet resistance ∼10 Ω cm^2). The resulting photoelectrodes were sintered at 450 °C, to obtain good mechanical and electrical contact at the interfaces of TiO_2/TiO_2 and TiO_2/substrate. Before deposition of the TiO_2 pastes, the FTO substrates were coated by a compact layer of TiO_2 deposited by spray pyrolisis (∼100 nm thick). These electrodes were calcinated at 450 °C for 30 min.

Electrode Sensitization. TiO_2 nanostructured electrodes were sensitized by CdS/CdSe QDs directly grown on the photoelectrode surface. In order to accomplish CdS sensitization by the successive ionic liquid adsorption and reaction (SILAR) method, Cd^{2+} ions were deposited from an ethanolic 0.05 M solution of $Cd(NO_3)_2{\cdot}4H_2O$. The sulfide source was a 0.05 M solution of $Na_2S{\cdot}9H_2O$ in methanol/water (50/50 v/v). A single CdS SILAR cycle consisted of 1 min of dip-coating of the TiO_2 working electrode into the metal precursors and subsequently into the sulfide solutions. After each bath, the photoanode is thoroughly rinsed by immersion in the corresponding solvent to remove the chemical residuals from the surface and subsequently dried with a N_2 gun. Four SILAR cycles was performed for CdS QD deposition. The CdSe deposition after CdS coating was performed by the chemical bath deposition (CBD) method. The CBD process was carried out as previously described:[11] a 80 mM sodium selenosulfate (Na_2SeSO_3) solution was prepared by refluxing elemental Se and Na_2SO_3 in Milli-Q water at 80 °C for 6 h with N_2 flux. The chemical bath solution was prepared by mixing 80 mM $CdSO_4$ and 80 mM Na_2SeSO_3 solutions with 120 mM nitriloacetic acid. The sensitized TiO_2 electrodes were immersed in the chemical bath solution at 10 °C for 12 h. Then, the electrodes were washed with Milli-Q water and dried with a N_2 gun. It is well known that a seed layer of CdS significantly enhances the growth rate of CdSe, producing an increase of the light absorption for the same CBD deposition time. In order to improve the stability and performance of all electrodes, they were covered with a ZnS protective coating, by twice dipping alternatively into 0.1 M $Zn(CH_3COO)_2$ and 0.1 M Na_2S solutions for 1 min/dip, rinsing with Milli-Q ultrapure water between dips.[36,37]

CE Preparation. Natural graphite powder (Fluka Company) was utilized to prepare graphite oxide suspension by a modified Hummers' method.[38,39] In a typical procedure, first, 0.5 g of graphite and 0.5 g of $NaNO_3$ were added in 23 mL of H_2SO_4. Then, the mixture was stirred in an ice bath for 10 min. After that, 3.0 g of potassium permanganate ($KMnO_4$) was slowly added to the suspension while it warmed to room temperature. The suspension was stirred continuously in a water bath for 2 h at 35 °C. Then, the prepared suspension was diluted by 40 mL of deionized (DI) water. During the diluting, the temperature of the suspension was maintained at less than 60 °C. Finally, 100 mL of DI water with 3 mL of H_2O_2 (30%) was added to the suspension in order to reduce residual permanganate to soluble manganese ions, corresponding to stopping the gas evolution of the suspension. The residual acids and salts of the graphite oxide suspension were removed by filtering through an anodic membrane filter (47 mm in diameter, 0.2 μm pore size; Whatman). The filtered graphite oxide powder was dispersed in DI water to obtain an aqueous graphite oxide suspension with a yellowish-brown color. Then, the aqueous suspension was centrifuged by an Eppendorf 5702 centrifuge with a rotor radius of 10 cm at 2000 rpm for 15 min and subsequently 8000 rpm for 10 min to remove any unexfoliated graphitic plates and tiny graphite particles, respectively. Finally, graphene oxide (GO) nanosheets were obtained by ultrasonication of the filtered graphite oxide suspension at a frequency of 40 kHz and power of 100 W for 30 min. The GO suspension (0.5 mg/mL) was spin coated with 2000 rpm on FTO substrates. In order to obtain full coverage of the FTO substrate, the spin-coating process was done three times. Between every spin-coating process, the FTO

dx.doi.org/10.1021/ph400011z | ACS Photonics 2014, 1, 323−330

substrates were subjected to hydrazine vapor at 120 °C for 1 h in order to reduce the GO-deposited sheets to reduced graphene oxide (RGO).

PbS counter electrodes were prepared by *in situ* deposition of PbS QDs on FTO substrates by the SILAR method. The as-cleaned FTO electrodes were successively immersed in two different precursors for 1 min, respectively. The first one consisted of 0.02 M $Pb(NO_3)_2$ dissolved in methanol, and the second solution consisted of 0.02 M Na_2S in methanol. Following each immersion, rinsing was performed for 1 min in pure methanol to remove the excess of each precursor solution. After that, samples were dried with a N_2 gun. This immersion cycle was repeated eight times. G/PbS composite electrodes were prepared by *in situ* deposition of PbS QDs on G-coated FTO glass by the SILAR method. Eight SILAR cycles were performed to deposit the PbS QDs on G-coated FTO electrodes. The Cu_2S counter electrodes were prepared by immersing a metallic brass substrate in HCl solution at 70 °C for 5 min and subsequently dipping it into a polysulfide solution for 10 min, resulting in a porous Cu_2S electrode.

QDSC Preparation. The solar cells were prepared by sandwiching various counter electrodes and a QD-sensitized photoelectrode using a spacer (thickness 50 μm) and permeating it with polysulfide electrolyte. The polysulfide electrolyte was a 1 M Na_2S, 1 M S, and 0.1 M NaOH solution in Milli-Q ultrapure water. The geometric area of the cells was 0.28 cm^2.

Materials and Solar Cell Characterization. Atomic force microscopy (AFM) images were obtained by using a Park Scientific CP-Research model (VEECO) with a Si tip (with a tip radius of 10 nm) in tapping mode (with a frequency of 320 kHz). Samples for AFM imaging were prepared by drop casting a diluted GO suspension (0.01 mg/mL) onto a cleaned Si(100) substrate. Raman spectroscopy (HR-800 Jobin-Yvon) was performed at room temperature using a Nd−YAG excitation source operating at a wavelength of 532 nm. To measure *I*−*V* characteristics of the graphene nanosheets, first, the graphene sheets were deposited between two Au electrodes (deposited on a Si/SiO_2 substrate by using e-beam evaporation) by drop casting the corresponding graphene suspension. The width of the electrodes was 120 μm, and the average distance between them was about 0.5 μm. The prepared electrode samples were dried under vacuum (with a pressure of ∼0.8 Pa) at 200 °C for 30 min. The number of graphene sheets deposited between the two electrodes was counted by an optical microscope. *I*−*V* curves were obtained by using a Keithley 485 auto ranging pico-ammeter. Impedance spectroscopy (IS) measurement and applied bias voltage decay (ABVD) were carried out with an FRA-equipped PGSTAT-30 potentiostat from Autolab. *J*−*V* measurements were carried out using a mask (0.24 cm^2). Cells were illuminated using a solar simulator at AM1.5 G, where the light intensity was adjusted to one sun intensity (100 mW/cm^2). Impedance spectroscopy measurements were carried out in dark conditions applying a 20 mV ac signal with the frequency ranging between 400 kHz and 0.1 Hz at different forward biases.

RESULTS AND DISCUSSION

Figure 1a shows the AFM image from the GO nanosheets deposited on the Si substrate. The height profile diagram of the AFM image indicated a thickness of ∼0.9 nm for our prepared GO layer, which is in good agreement with the typical thicknesses reported for single-layer GO sheets.

Since Raman spectroscopy is a powerful technique for distinguishing the single- and multilayer characteristics of

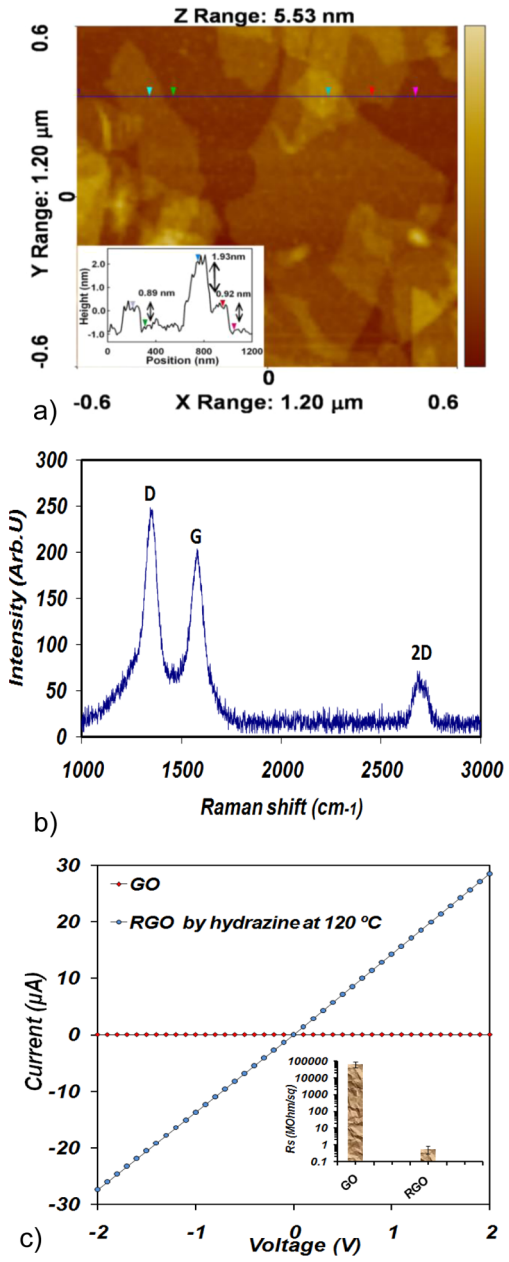

Figure 1. (a) AFM image of GO sheets with corresponding profile diagram in the inset. (b) Raman spectrum from GO sheets and (c) *I*−*V* diagram of the as-prepared GO sheets and the GO sheets reduced by hydrazine at 120 °C. The inset shows electrical sheet resistance of the GO and the reduced GO sheets obtained from the corresponding *I*−*V* curves.

graphene layers, we studied Raman characteristic peaks of the GO sheets, as shown in Figure 1b. The common characteristics of carbon materials in Raman spectra are the G line (∼1580 cm^{-1}) related to the first-order scattering of the E_{2g} phonons of sp^2 carbon atoms and the D line (∼1350 cm^{-1}) as a breathing mode of κ-point phonons of A_{1g} symmetry, which were assigned to structural imperfections induced by the attachment of hydroxyl and/or epoxide groups on the carbon surface.[40] In fact, the D line indicates a decrease in size of the in-plane sp^2 domains and formation of sp^3 bonds due to oxidation. Moreover, the D line can be related to disorders (such as vacancies and grain boundaries), edges, and amorphous carbon species.[41] In addition to the G line, the 2D line of Raman spectra of graphene-based

dx.doi.org/10.1021/ph400011z | ACS Photonics 2014, 1, 323−330

materials (explained by the adopted double resonant model[42]) are very sensitive to the number of graphene layers and stacking order along the out-of-plane axis of the layers.[43] The 2D peak of the single-layer graphene sheets shows usually a Lorentzian form centered at 2679 cm^{-1}, while the 2D band of the multilayer (2−4 layers) sheet exhibits more broadened peaks with a shift to higher wave numbers by 19 cm^{-1}. In this work, Figure 1b shows that the 2D band of the as-prepared GO sheets was centered at about 2680 cm^{-1} with a low-intensity shoulder at the higher wave numbers. Thus, single-layer GO sheets were present in the as-prepared GO suspension.

The effect of the reduction processes on the $I-V$ characteristics of the GO sheets is presented in Figure 1c. The linear form of the $I-V$ curves implied the metallic property of the sheets and formation of ohmic contact between the graphene sheets and the Au electrodes. Using the slope of the $I-V$ curves and by knowing the number of sheets connected to the electrodes, electrical sheet resistance (R_s) of the graphene sheets was evaluated, as shown in the inset of Figure 3c. The R_s of the as-prepared GO sheets was considerably high, 1.3×10^9 Ω/sq, and it was substantially decreased to 5.8×10^5 Ω/sq, indicating the effective reduction of the GO suspension by hydrazine at 120 °C. Three kinds of counter electrodes containing FTO/G, FTO/PbS, and FTO/G/PbS were prepared as explained in the Experimental Section. A schematic structure of the prepared counter electrodes is shown in Figure 2. Additionally, a conventional Cu_2S counter electrode was fabricated as a reference to compare the cells with conventional QDSCs.

QDSCs were assembled as explained in the Experimental Section, and their photovoltaic properties were investigated. Current−voltage curves of the cells are presented in Figure 3.

Table 1 shows the solar cell parameters obtained for these QDSCs: photocurrent J_{sc}, open-circuit voltage V_{oc}, fill factor FF, and efficiency η, which are tested under standard conditions (100 mW/cm^2 AM 1.5G).

As it can be seen from Table 1, cells with G and PbS counter electrodes show low efficiencies, 0.23% and 1.28%, respectively, which is mainly caused by the low fill factors in these cells. From the results, it seems that these electrodes have not exhibited considerable catalytic activity in redox polysulfide electrolytes. According to Table 1, considerable improvement in cell efficiencies (2.63%) has been obtained by integrating the G and PbS quantum dots on the FTO substrate. Especially the fill factor (0.42) has increased in comparison to G (0.12) and PbS (0.23) CEs. The fill factor of cells with G/PbS counter electrodes is comparable to that of Cu_2S (0.46), which indicates the good catalytic activity of G/PbS in redox polysulfide electrolytes.

Figure 4 shows the SEM micrograph of the various synthesized CEs. Figure 4a shows the porous structure of a Cu_2S CE that is made on a brass substrate. Figure 4b indicates the PbS nanoparticles that are deposited on an FTO glass substrate by the SILAR method. PbS nanoparticles are almost tightly connected together and have made a layer with low porosity (Figure 4b) in comparison to Cu_2S CEs (Figure 4a). The structure of the G/PbS composite electrodes is shown in Figure 4c,d. As it can be seen in Figure 4c, conducting graphene sheets are decorated by catalytic PbS nanoparticles. Here, micrometer-sized graphene sheets with PbS nanoparticles make a three-dimensional porous network that could enhance the redox electrolyte diffusion through it.

To better understand the physical characteristics of these cells, impedance spectroscopy measurements and ABVD were carried out on QDSCs. Chemical capacitance, C_μ (Figure 5a), and

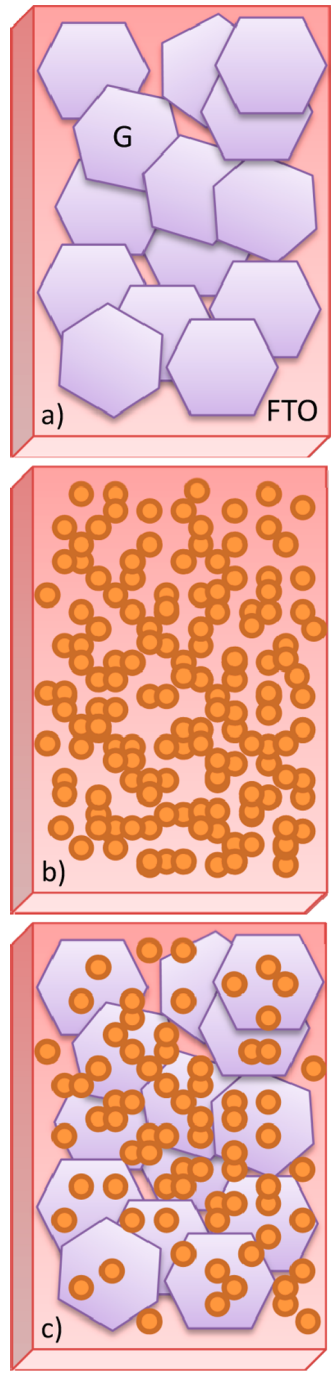

Figure 2. Schematic structure of the prepared counter electrodes: FTO/G (a), FTO/PbS (b), FTO/G/PbS (c).

recombination resistance, R_{rec} (Figure 5b), have been obtained from IS measurements using the previously developed model.[44,45] C_μ is plotted against the voltage drop in the sensitized electrode, V_F. V_F was obtained by subtracting the voltage drop of the series resistance, V_{series} (contacts, counter electrode, electrolyte diffusion), by $V_F = V_{app} - V_{series}$, where V_{app} is the applied potential in the IS measurements. R_{rec} is plotted against the voltage drop in a common equivalent conduction band (CB), V_{ecb}, where the effect of different TiO_2 CBs between samples is removed.[45] Plotting R_{rec} against the V_{ecb} allows an analysis of the recombination resistance on the basis of an equal density of electrons n (i.e., the same distance between the electron Fermi level and the TiO_2 CB). This procedure is carried out by shifting

dx.doi.org/10.1021/ph400011z | ACS Photonics 2014, 1, 323−330

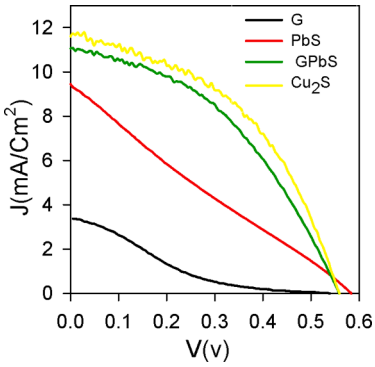

Figure 3. Current–voltage characteristic of cells with G, PbS, G/PbS, and Cu_2S counter electrodes.

Table 1. Photovoltaic Parameters of QDSCs Prepared and Analyzed: Photocurrent J_{sc}, Open-Circuit Voltage V_{oc}, Fill Factor FF, and Efficiency η, as a Function of the Different Cell Counter Electrodes, Tested under Standard Light Illumination Conditions (100 mW/cm^2 AM 1.5G)

counter type	V_{oc} (mV)	J_{sc}(mA/cm^2)	FF	E (%)
G	539	3.42	0.12	0.23
PbS	583	9.47	0.23	1.28
G/PbS	559	11	0.42	2.63
Cu_2S	564	11.6	0.46	3.01

V_F until the chemical capacitance overlaps. The methods to obtain the dependences on V_F and V_{ecb} from IS measurements have been previously reported.[45−47]

Considering the chemical capacitance (Figure 5a), all the samples show similar slopes for C_μ, indicating a similar density of states.[45] On the other hand, C_μ is shifted in the case of cells with G CE, indicating that there is an upward displacement of the TiO_2 CB that can potentially increase the open-circuit photovoltage.[22] On the other hand, according to Figure 5b, cells with G CE have very low recombination resistance (high recombination rate), which has led to low open-circuit photovoltage in these cells in spite of the CB upward shift (Table 1). From Figure 5b it can be indicated that cells with PbS CE have the highest recombination resistance (lower recombination). This higher recombination resistance arises from the lower dark current obtained for these cells; see Figure 6a. According to Table 1, cells with PbS CE have the maximum open-circuit photovoltage, which arises from the higher recombination resistance in these cells.

In addition, the higher recombination resistance of the cells with PbS CE has been confirmed comparing the electron lifetime, τ_n, of the samples, Figure 6b. τ_n has been measured by ABVD, under dark conditions.[48] Conversely, the cells with the higher recombination resistance (cells with PbS and G/PbS CEs) show longer electron lifetime than cells with G and Cu_2S CEs. This fact points out the crucial role of recombination on the QDSC performance. In spite of the higher recombination resistance (Figure 5b) and consequently higher open-circuit photovoltage (Table 1), in cells with PbS CEs, current density and especially fill factor are lower than in G/PbS and Cu_2S CE cells (Table 1). To further elucidate the catalytic activities of different CEs and their impact on the fill factors, EIS experiments were carried out using symmetric cells fabricated with two identical electrodes (CE/electrolyte/CE). From the IS measurement of symmetric cells, the series resistance (R_s) and the charge-

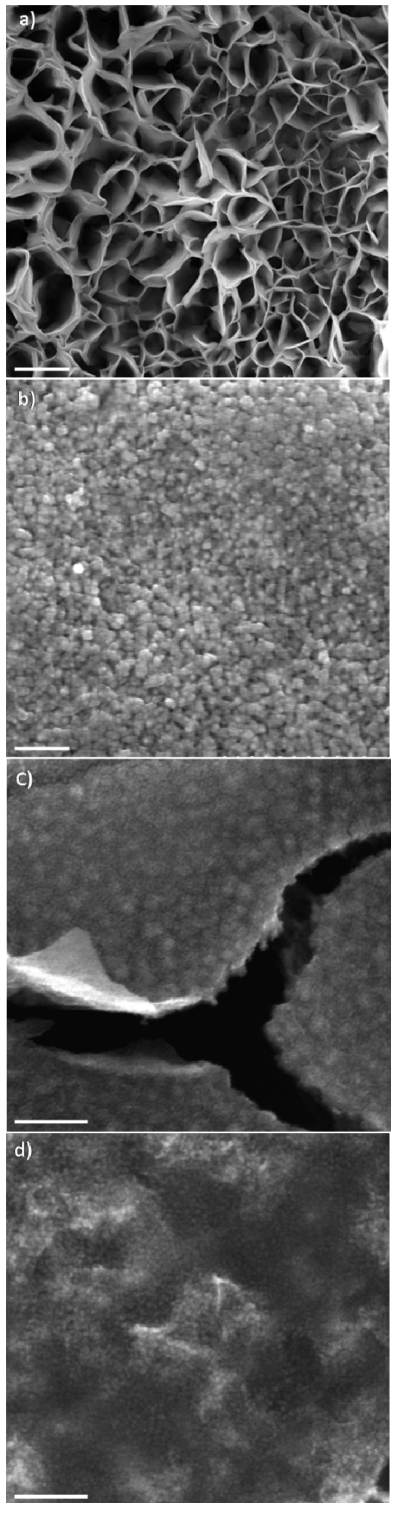

Figure 4. SEM micrograph of various counter electrodes: (a) Cu_2S (scale bar: 2 μm), (b) PbS (scale bar: 150 nm), (c, d) G/PbS (scale bar: 400 nm).

transfer resistance (R_{ct}) at the CE/electrolyte interface were measured (Table 2).

The R_{ct} increases in the order Cu_2S (2.8 Ω cm^2) < G/PbS (4.13 Ω cm^2) < PbS (7.78 Ω cm^2) < G (10.63 Ω cm^2), indicating an inverse order of catalytic activity on the reduction of oxidized redox polysulfide species. Considerable obscurity in charge transfer at the CE/electrolyte interface increases internal

dx.doi.org/10.1021/ph400011z | ACS Photonics 2014, 1, 323−330

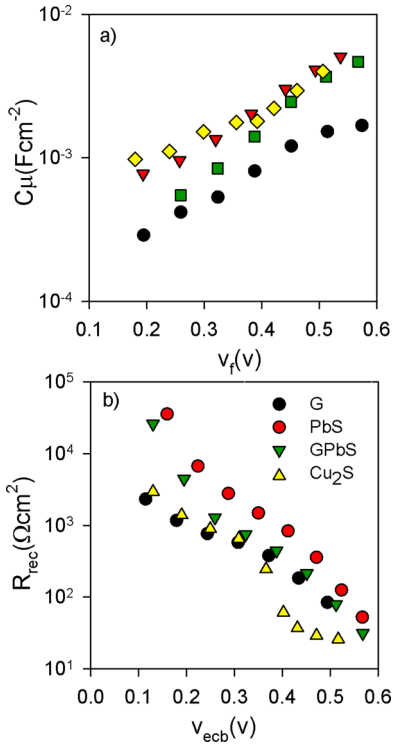

Figure 5. Chemical capacitance and recombination resistance for QDSCs with G, PbS, G/PbS, and Cu_2S CEs: (a) chemical capacitance, (b) recombination resistance. Chemical capacitance and recombination resistance have been obtained from IS measurements.

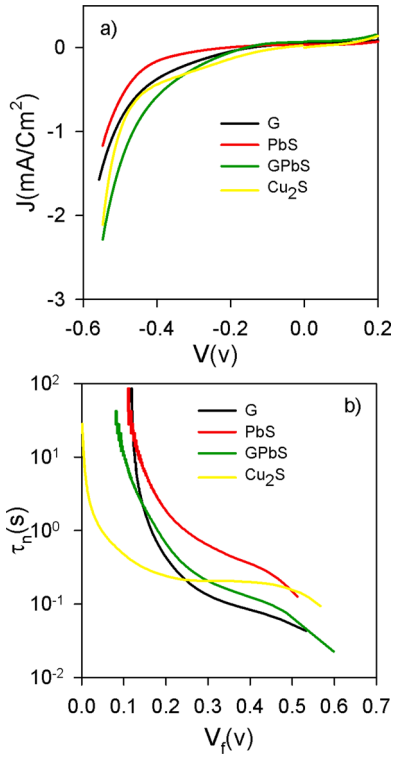

Figure 6. Dark current and electron lifetime for QDSCs with various CEs: (a) dark current and (b) electron lifetime. Electron lifetime has been obtained from ABVD measurements.[48]

resistances and concentration gradients of the redox species in the electrolyte, parameters that strongly affect the fill factor. One can see that the use of G as a CE strongly decreased the fill factor; see Table 1. Our results show that graphene has a poor catalytic activity in polysulfide electrolytes, while the catalytic activity has improved in the case of PbS CEs. According to Table 1, considerable improvement in QDSC efficiency and especially fill factors can be obtained by applying the G/PbS composite CEs in cells, which indicates the good catalytic activity of these composite electrodes in polysulfide electrolytes. It is noticeable that the fill factor of cells with G (0.12) and PbS (0.23) CEs has considerably improved by just compositing these materials in a G/PbS structure (fill factor: 0.42).

Table 2. Series Resistance (R_s) and the Charge Transfer Resistance (R_{ct}) at the CE/Electrolyte Interface Measured by IS

counter type	R_s (Ω cm^2)	R_{ct} (Ω cm^2)
G	9.31	10.63
PbS	9.42	7.78
G/PbS	10.26	4.13
Cu_2S	6.23	2.80

As it was explained before, parameters such as CE conductivity, catalytic activity, and the effective interface area between the CE and redox electrolyte,have considerable influence on the CE performance. It is known that graphene has a poor catalytic activity in polysulfide electrolytes, in spite of its good conductivity, and some kind of surface functionalization or decoration with catalytic QDs can improve its catalytic properties.[49−51] As it can be seen from our results (Table 2), a high charge-transfer resistance (R_{ct}) at the graphene CE/electrolyte interface (R_{ct} = 10.63 Ωcm^2) was obtained, which led to a poor catalytic activity and consequently a low fill factor according to Table 1. As it was explained before, PbS CEs are made by a continuous layer of PbS nanoparticles on an FTO substrate with a lower porosity in comparison to conventional porous Cu_2S CEs (Figure 4a and b). The continuous layer of PbS nanoparticles on an FTO substrate, in spite of increasing the CE conductivity, remarkably reduces the effective electrolyte/CE interface area. The lower effective interface area decreases the catalytic activity of the CE noticeably in comparison with more porous structures like Cu_2S CEs. As it can be seen from Table 2, a PbS CE has a considerably higher charge-transfer resistance (R_{ct}) at the CE/electrolyte interface (R_{ct} = 7.78 Ω cm^2) than Cu_2S (R_{ct} = 2.8 Ω cm^2). The high value of R_{ct} in the PbS CE confirms its low catalytic activity owing to its low effective interface area with the electrolyte. As it can be seen from Table 1, the cells with a PbS CE have a lower fill factor and efficiency in comparison to the cells with a Cu_2S CE.

In the G/PbS CEs two-dimensional graphene sheets provide considerable contact surface area with the FTO glass substrate, which can enhance the electron transport to the sulfide-active PbS catalyst sites. On the other hand, in the G/PbS structure, each graphene sheet provides a large surface area for catalytic PbS nanoparticle nucleation and growth. Most importantly here in contrast with PbS CEs that have a layer of PbS nanoparticles with low porosity (Figure 4b), micrometer-sized graphene sheets with PbS nanoparticles make a three-dimensional porous structure (Figure 4c) that enhances the effective electrolyte/CE interface area in comparison to G or PbS CEs. As it can be seen from Table 2, the charge-transfer resistance (R_{ct}) at the graphene, PbS, and G/PbS CE/electrolyte is 10.63, 7.78, and 4.13 Ω cm^2, respectively, which confirms the considerable improvement in G/PbS over G and PbS. According to Table 2, the charge-transfer

dx.doi.org/10.1021/ph400011z | ACS Photonics 2014, 1, 323−330

resistance (R_{ct}) at the Cu_2S CE/electrolyte is 2.8 Ω cm^2, which is a little lower than the G/PbS CE (4.13 Ω cm^2), and consequently superior catalytic activity is expected for Cu_2S. Figure 4a shows the Cu_2S highly porous structure, which enhances the redox electrolyte/CE interface area and leads to good catalytic activities. It is noticeable that in spite of the good catalytic property that was obtained for Cu_2S, the method of Cu_2S synthesis on a metallic brass substrate is not easy and cost-effective (see Experimental Section). More importantly sealing the metallic CE with the photoanode electrode that is made on the FTO glass substrate is a challenge. This is especially a serious problem for large-scale production. Here in comparison to making Cu_2S CEs on metallic substrates, we have made G/PbS CEs on an FTO glass substrate with simple and cost-effective chemical methods. As a first report of a new kind of CEs for QDSCs, the catalytic activity of this CE was noticeable. The fill factor of the cells with G/PbS CEs was obtained as 0.42, in comparison with optimized Cu_2S CEs with a 0.46 fill factor (Table 1). It is noticeable that the fill factor of cells with G/PbS CEs is more than 90% of that of the optimized Cu_2S CEs for the first report of this kind of CE without further optimization. According to Table 1, the efficiency of the cells with the new G/PbS CE was obtained as 2.63%, which is near 88% of the cells' efficiency with Cu_2S CEs. Desirable G/PbS catalytic properties that were obtained here and the simple and cost-effective chemical methods of G/PbS synthesis in comparison to Cu_2S indicate the potential application of graphene/noble metal sulfide composite electrodes in making efficient QDSCs in the near future.

CONCLUSIONS

We have successfully made G/PbS composite counter electrodes for CdS/CdSe QDSCs by *in situ* deposition of PbS QDs on graphene sheets with the SILAR method. We have shown that catalytic activity of bare G and PbS CEs in a polysulfide redox electrolyte can be considerably enhanced by compositing these structures to make G/PbS CEs. For the first reported CdS/CdSe-sensitized cell with the G/PbS CE, a cell performance with 2.63% efficiency (V_{oc} = 559 mV, J_{sc} = 11 mA/cm^2, FF = 0.42) was obtained, which is comparable with the photovoltaic properties of the cells with optimized conventional Cu_2S CEs (η = 3.01%, V_{oc} = 564 mV, J_{sc} = 11.6 mA/cm^2, FF = 0.46). To better understand the physical characteristics of these solar cells, impedance spectroscopy and ABVD were carried out on QDSCs. It was shown that the efficiency of the QDSCs can be potentially improved by using more catalytic counter electrodes in redox polysulfide electrolytes. Our results indicate the potential application of graphene and noble metal sulfide composite electrodes in high-efficiency QDSCs.

AUTHOR INFORMATION

Corresponding Authors

*E-mail: samadpour@kntu.ac.ir.

*E-mail: iraji@sharif.edu.

Notes

The authors declare no competing financial interest.

REFERENCES

(1) Hodes, G. Comparison of dye and semiconductor-sensitized porous nanocrystalline liquid junction solar cells. *J. Phys. Chem. C* **2008**, *112*, 17778−17787.

(2) Kamat, P. V. Quantum dot solar cells. Semiconductor nanocrystals as light harvesters. *J. Phys. Chem. C* **2008**, *112*, 18737−18753.

(3) Kamat, P. V.; Tvrdy, K.; Baker, D. R.; Radich, J. G. Beyond photovoltaics: Semiconductor nanoarchitectures for liquid-junction solar cells. *Chem. Rev.* **2010**, *110*, 6664−6688.

(4) Mora-Seró, I.; Bisquert, J. Breakthroughs in the development of semiconductor-sensitized solar cells. *J. Phys. Chem. Lett.* **2010**, *1*, 3046−3052.

(5) Mora-Seró, I.; Giménez, S.; Fabregat-Santiago, F.; Gómez, R.; Shen, Q.; Toyoda, T.; Bisquert, J. Recombination in quantum dot sensitized solar cells. *Acc. Chem. Res.* **2009**, *42*, 1848−1857.

(6) Samadpour, M.; Boix, P. P.; Giménez, S.; Iraji Zad, A.; Taghavinia, N.; Mora-Seró, I.; Bisquert, J. Fluorine treatment of TiO_2 for enhancing quantum dot sensitized solar cell performance. *J. Phys. Chem. C* **2011**, *115* (29), 14400−14407.

(7) Samadpour, M.; Irajizad, A.; Taghavinia, N.; Molaei, M. A new structure to increase the photostability of CdTe quantum dot sensitized solar cells. *J. Phys. D: Appl. Phys.* **2011**, *44* (4), 045103.

(8) Zhang, Q.; Guo, X.; Huang, X.; Huang, S.; Li, D.; Luo, Y.; Shen, Q.; Toyoda, T.; Meng, Q. Highly efficient CdS/CdSe-sensitized solar cells controlled by the structural properties of compact porous TiO_2 photoelectrodes. *Phys. Chem. Chem. Phys.* **2011**, *13*, 4659−4667.

(9) Sudhagar, P.; Song, T.; Lee, D. H.; Mora-Seró, I.; Bisquert, J.; Laudenslager, M.; Sigmund, W. M.; Park, W. I.; Paik, U.; Kang, Y. S. High open circuit voltage quantum dot sensitized solar cells manufactured with ZnO nanowire arrays and Si/ZnO branched hierarchical structures. *J. Phys. Chem. Lett.* **2011**, *2*, 1984−1990.

(10) Samadpour, M.; Giménez, S.; Iraji-Zad, A.; Taghavinia, N.; Mora-Seró, I. Easily manufactured TiO_2 hollow fibers for quantum dot sensitized solar cells. *J. Phys. Chem. Chem. Phys.* **2012**, *14*, 522−528.

(11) Samadpour, M.; Giménez, S.; Boix, P. P.; Shen, Q.; Calvo, M. E.; Taghavinia, N.; Iraji zad, A.; Toyoda, T.; Míguez, H.; Mora-Seró, I. Effect of nanostructured electrode architecture and semiconductor deposition strategy on the photovoltaic performance of quantum dot sensitized solar cells. *Electrochim. Acta* **2012**, *75*, 139−147.

(12) Lee, Y. L.; Lo, Y. S. Highly efficient quantum-dot-sensitized solar cell based on co-sensitization of CdS/CdSe. *Adv. Funct. Mater.* **2009**, *19*, 604−609.

(13) Kongkanand, A.; Tvrdy, K.; Takechi, K.; Kuno, M.; Kamat, P. V. Quantum dot solar cells. Tuning photoresponse through size and shape control of CdSe-TiO_2 architecture. *J. Am. Chem. Soc.* **2008**, *130*, 4007−4015.

(14) Robel, I.; Subramanian, V.; Kuno, M.; Kamat, P. V. Quantum dot solar cells. Harvesting light energy with CdSe nanocrystals molecularly linked to mesoscopic TiO_2 films. *J. Am. Chem. Soc.* **2006**, *128* (7), 2385−2393.

(15) Lee, H. J.; Chen, P.; Moon, S.-J.; Sauvage, F.; Sivula, K.; Bessho, T.; Gamelin, D. R.; Comte, P.; Zakeeruddin, S. M.; Seok, S. I.; Grätzel, M.; Nazeeruddin, M. K. Regenerative PbS and CdS quantum dot sensitized solar cells with a cobalt complex as hole mediator. *Langmuir* **2009**, *25*, 7602−7608.

(16) Lee, Y. L.; Chang, C. H. Efficient polysulfide electrolyte for CdS quantum dot-sensitized solar cells. *J. Power Sources* **2008**, *185*, 584−588.

(17) Li, L.; Yang, X.; Gao, J.; Tian, H.; Zhao, J.; Hagfeldt, A.; Sun, L. Highly efficient CdS quantum dot-sensitized solar cells based on a modified polysulfide electrolyte. *J. Am. Chem. Soc.* **2011**, *133*, 8458−8460.

(18) Yu, Z.; Zhang, Q.; Qin, D.; Luo, Y.; Li, D.; Shen, Q.; Toyoda, T.; Meng, Q. Highly efficient quasi-solid-state quantum-dot-sensitized solar cell based on hydrogel electrolytes. *Electrochem. Commun.* **2010**, *12*, 1776−1779.

(19) Jovanovski, V.; González-Pedro, V.; Giménez, S.; Azaceta, E.; Cabañero, G.; Grande, H.; Tena-Zaera, R.; Mora-Seró, I.; Bisquert, J. A sulfide/polysulfide-based ionic liquid electrolyte for quantum dot-sensitized solar cells. *J. Am. Chem. Soc.* **2011**, *133*, 20156−20159.

(20) Radich, J. G.; Dwyer, R.; Kamat, P. V. Cu_2S reduced graphene oxide composite for high-efficiency quantum dot solar cells. Overcoming the redox limitations of S^{2-}/S_n^{2-} at the counter electrode. *J. Phys. Chem. Lett.* **2011**, *2*, 2453−2460.

(21) Giménez, S.; Mora-Seró, I.; Macor, L.; Guijarro, N.; Lana-Villarreal, T.; Gómez, R.; Diguna, L. J.; Shen, Q.; Toyoda, T.; Bisquert, J.

Improving the performance of colloidal quantum-dot-sensitized solar cells. *Nanotechnology* **2009**, *20*, 295204.
(22) Gónzalez-Pedro, V.; Xu, X.; Mora-Seró, I.; Bisquert, J. Modeling high-efficiency quantum dot sensitized solar cells. *ACS Nano* **2010**, *4*, 5783−5790.
(23) Chiba, Y.; Islam, A.; Watanabe, Y.; Komiya, R.; Koide, N.; Han, L. Dye-sensitized solar cells with conversion efficiency of 11.1%. *Jpn. J. Appl. Phys. Part 2 Lett.* **2006**, *45*, L638.
(24) O'Regan, B.; Gratzel, M. A low-cost, high-efficiency solar cell based on dye-sensitized colloidal TiO_2 films. *Nature* **1991**, *353*, 737−740.
(25) Yang, Z.; Chen, C. Y.; Liu, C. W.; Li, C. L.; Chang, H. T. Quantum Dot-Sensitized Solar Cells Featuring CuS/CoS Electrodes Provide 4.1% Efficiency. *Adv. Energy Mater.* **2011**, *1*, 259−264.
(26) Deng, M.; Huang, S.; Zhang, Q.; Li, D.; Luo, Y.; Shen, Q.; Toyoda, T.; Meng, Q. Screen-printed Cu_2S-based counter electrode for quantum-dot-sensitized solar cell. *Chem. Lett.* **2010**, *39*, 1168−1170.
(27) Tachan, Z.; Shalom, M.; Hod, I.; Ruhle, S.; Tirosh, S.; Zaban, A. PbS as a highly catalytic counter electrode for polysulfide-based quantum dot solar cells. *J. Phys. Chem. C* **2011**, *115*, 6162−6166.
(28) Seol, M.; Ramasamy, E.; Lee, J.; Yong, K. Highly efficient and durable quantum dot sensitized ZnO nanowire solar cell using noble-metal-free counter electrode. *J. Phys. Chem. C* **2011**, *115*, 22018−22024.
(29) Fang, B.; Kim, M.; Fan, S. Q.; Kim, J. H.; Wilkinson, D. P.; Ko, J.; Yu, J. S. Facile synthesis of open mesoporous carbon nanofibers with tailored nanostructure as a highly efficient counter electrode in CdSe quantum-dot-sensitized solar cells. *J. Mater. Chem.* **2011**, *21*, 8742−8748.
(30) Santra, P. K.; Kamat, P. V. Mn-doped quantum dot sensitized solar cells: a strategy to boost efficiency over 5%. *J. Am. Chem. Soc.* **2012**, *134*, 2508−2511.
(31) Imoto, K.; Takahashi, K.; Yamaguchi, T.; Komura, T.; Nakamura, J. I.; Murata, K. High-performance carbon counter electrode for dye-sensitized solar cells. *Sol. Energy Mater. Sol. Cells* **2003**, *79* (4), 459−469.
(32) Chen, J.; Li, K.; Luo, Y.; Guo, X.; Li, D.; Deng, M.; Meng, Q. A flexible carbon counter electrode for dye-sensitized solar cells. *Carbon* **2009**, *47* (11), 2704−2708.
(33) Wang, G.; Xing, W.; Zhuo, S. Application of mesoporous carbon to counter electrode for dye-sensitized solar cells. *J. Power Sources* **2009**, *194* (1), 568−573.
(34) Sudhagar, P.; Ramasamy, E.; Cho, W. H.; Lee, J.; Kang, Y. S. Robust mesocellular carbon foam counter electrode for quantum-dot sensitized solar cells. *Electrochem. Commun.* **2011**, *13* (1), 34−37.
(35) Geim, A. K.; Novoselov, K. S. The rise of graphene. *Nat. Mater.* **2007**, *6* (3), 183−191.
(36) Lee, H. J.; Bang, J.; Park, J.; Kim, S.; Park, S. M. Multilayered semiconductor (CdS/CdSe/ZnS)-sensitized TiO_2 mesoporous solar cells: All prepared by successive ionic layer adsorption and reaction processes. *Chem. Mater.* **2010**, *22*, 5636−5643.
(37) Shen, Q.; Kobayashi, J.; Diguna, L. J.; Toyoda, T. Effect of ZnS coating on the photovoltaic properties of CdSe quantum dot-sensitized solar cells. *J. Appl. Phys.* **2008**, *103*, 084304.
(38) Hummers, W. S.; Offeman, R. E. Preparation of Graphitic Oxide. *J. Am. Chem. Soc.* **1958**, *80*, 1339.
(39) Kovtyukhova, N. I.; Ollivier, P. J.; Martin, B. R.; Mallouk, T. E.; Chizhik, S. A.; Buzaneva, E. V.; Gorchinskiy, A. D. Layer-by-layer assembly of ultrathin composite films from micron-sized graphite oxide sheets and polycations. *Chem. Mater.* **1999**, *11*, 771−778.
(40) Ferrari, A. C.; Robertson, J. Interpretation of Raman spectra of disordered and amorphous carbon. *Phys. Rev. B* **2000**, *61*, 14095−14107.
(41) Ferrari, A. C.; et al. Raman spectrum of graphene and graphene layers. *Phys. Rev. Lett.* **2006**, *97*, 187401−187405.
(42) Thomsen, C.; Reich, S. Double resonant Raman scattering in graphite. *Phys. Rev. Lett.* **2000**, *85*, 5214−5217.
(43) Malard, L. M.; Pimenta, M. A.; Dresselhaus, G.; Dresselhaus, M. S. Raman spectroscopy in graphene. *Phys. Rep.* **2009**, *473*, 51−87.
(44) Fabregat-Santiago, F.; Bisquert, J.; Garcia-Belmonte, G.; Boschloo, G.; Hagfeldt, A. Influence of electrolyte in transport and recombination in dye-sensitized solar cells studied by impedance spectroscopy. *Sol. Energy Mater. Sol. Cells* **2005**, *87*, 117−131.
(45) Fabregat-Santiago, F.; Garcia-Belmonte, G.; Mora-Seró, I.; Bisquert, J. Characterization of nanostructured hybrid and organic solar cells by impedance spectroscopy. *Phys. Chem. Chem. Phys.* **2011**, *13*, 9083−9118.
(46) Barea, E. M.; Shalom, M.; Giménez, S.; Hod, I.; Mora-Seró, I.; Zaban, A.; Bisquert, J. Design of injection and recombination in quantum dot sensitized solar cells. *J. Am. Chem. Soc.* **2010**, *132*, 6834−6839.
(47) Braga, A.; Giménez, S.; Concina, I.; Vomiero, A.; Mora-Seró, I. Panchromatic sensitized solar cells based on metal sulfide quantum dots grown directly on nanostructured TiO_2 electrodes. *J. Phys. Chem. Lett.* **2011**, *2*, 454−460.
(48) Bisquert, J.; Zaban, A.; Greenshtein, M.; Mora-Seró, I. Determination of rate constants for charge transfer and the distribution of semiconductor and electrolyte electronic energy levels in dye-sensitized solar cells by open-circuit photovoltage decay method. *J. Am. Chem. Soc.* **2004**, *126*, 13550−13559.
(49) Bay, L.; West, K.; Winther-Jensen, B.; Jacobsen, T. Electrochemical reaction rates in a dye-sensitized solar cell - the iodide/triiodide redox system. *Sol. Energy Mater. Sol. Cells* **2006**, *90*, 341−351.
(50) Cruz, R.; Pacheco Tanaka, D. A.; Mendes, A. Reduced graphene oxide films as transparent counter-electrodes for dye-sensitized solar cells. *Sol. Energy* **2012**, *86*, 716−724.
(51) Kavan, L.; Yum, J. H.; Gratzel, M. Optically transparent cathode for dye-sensitized solar cells based on graphene nanoplatelets. *ACS Nano* **2011**, *5*, 165−172.